applied sciences

MDPI

Article

Behaviour of Compacted Filtered Iron Ore Tailings–Portland Cement Blends: New Brazilian Trend for Tailings Disposal by Stacking

Nilo Cesar Consoli [1,*], Jordanna Chamon Vogt [2], João Paulo Sousa Silva [3], Helder Mansur Chaves [1], Hugo Carlos Scheuermann Filho [1], Eclesielter Batista Moreira [1] and Andres Lotero [1]

1 Graduate Program in Civil Engineering, Universidade Federal do Rio Grande do Sul, Porto Alegre 90035-190, Brazil; heldermansurchaves@hotmail.com (H.M.C.); hugocsf@gmail.com (H.C.S.F.); eclesielter_ebm@hotmail.com (E.B.M.); andreslotero@hotmail.com (A.L.)
2 Coproducts Business Development, VALE S.A., Nova Lima 34000-000, Brazil; jordanna.vogt@vale.com
3 Exploration and Mineral Projects—Mineral Development Centre, VALE S.A., Santa Luzia 33040-900, Brazil; joao.paulo.silva@vale.com
* Correspondence: consoli@ufrgs.br

Citation: Consoli, N.C.; Vogt, J.C.; Silva, J.P.S.; Chaves, H.M.; Scheuermann Filho, H.C.; Moreira, E.B.; Lotero, A. Behaviour of Compacted Filtered Iron Ore Tailings–Portland Cement Blends: New Brazilian Trend for Tailings Disposal by Stacking. *Appl. Sci.* **2022**, *12*, 836. https://doi.org/10.3390/app12020836

Academic Editors: Paulo José da Venda Oliveira and António Alberto Santos Correia

Received: 29 November 2021
Accepted: 9 January 2022
Published: 14 January 2022

Abstract: Failures of tailings dams, primarily due to liquefaction, have occurred in Brazil in recent years. These events have prompted the Brazilian government to place restrictions on the construction of new dams, as iron ore tailings deposited behind upstream dams by spigotting have been shown to have low in situ densities and strengths and are prone to failure. This work proposes a new trend for tailings disposal: stacking compacted filtered ore tailings–Portland cement blends. As part of the proposal, it analyses the behaviour of compacted iron ore tailings–Portland cement blends, considering the use of small amounts of Portland cement under distinct compaction degrees. With the intention of evaluating the stress–strain–strength–durability behaviour of the blends, the following tests were carried out: unconfined compression tests; pulse velocity tests; wetting–drying tests; and standard drained triaxial compression tests with internal measurement of strains. This is the first study performed to determine the strength and initial shear stiffness evolution of iron ore tailings–Portland cement blends during their curing time, as well friction angle and cohesion intercept. This manuscript postulates an analysis of original experimental results centred on the porosity/cement index (η/Civ). This index can help select the cement quantity and density for important design parameters of compacted iron ore tailings–cement blends required in geotechnical engineering projects such as the proposed compacted filtered iron ore tailings–cement blends stacking.

Keywords: cemented iron ore tailings behaviour; filtered tailings stacking; Portland cement; compaction

1. Introduction

Tailings are the residues derived from ore extraction and processing and are mainly constituted by crushed rock fines, chemicals and water [1,2]. This combination results in a material having an aqueous slurry consistency which facilitates the disposal in large impoundments designated as tailings dams. In this regard, the upstream method of construction (Figure 1a) is the cheapest manner to expand the dam once the initial embankment has been built. In brief, this methodology consists in founding the raising dam directly into the deposited tailings. Nonetheless, as the tailings are customarily found saturated at a loose condition, stability issues related to static and/or dynamic liquefaction may compromise the security of the dams assembled using the upstream method [3,4].

For this reason, since 2019, building upstream tailings dams has been prohibited in Brazil due to collapses that released massive mudslides that buried the surrounding areas, resulting in destruction, environment pollution and several deaths. According to the non-profit organization World Mine Tailings Failures [5], 45 tailings dam failures occurred between 2009 and 2019. A United Nations Environment Programme [6] report documented some of these significant failures, if not in terms of loss of life, then in terms of environmental damage. These are some of the incidents which occurred between 2015 and 2020: Fundão, 2015 (Brazil); New Walles, 2016 (USA); Tonglushan, 2017 (China); Mishor Rotem, 2017 (Israel); Brumadinho, 2019 (Brazil); and Hpakant, 2020 (Myanmar), among others [7,8].

Numerous other tailings failures have occurred worldwide but were not reported as they did not involve any fatalities. These catastrophic incidents may be caused, in many cases, by lack of control of the design, but to some extent they reflect a relatively poor understanding of the mechanics of tailings. Santamarina et al. [9] highlight how knowledge gaps and management shortcomings contribute to the catastrophic failures that claim thousands of lives around the world. Therefore, a deeper knowledge on the behaviour of these structures and materials, as well as the search for alternatives focusing risk mitigation, is crucial and of great concern to companies, government agencies and society.

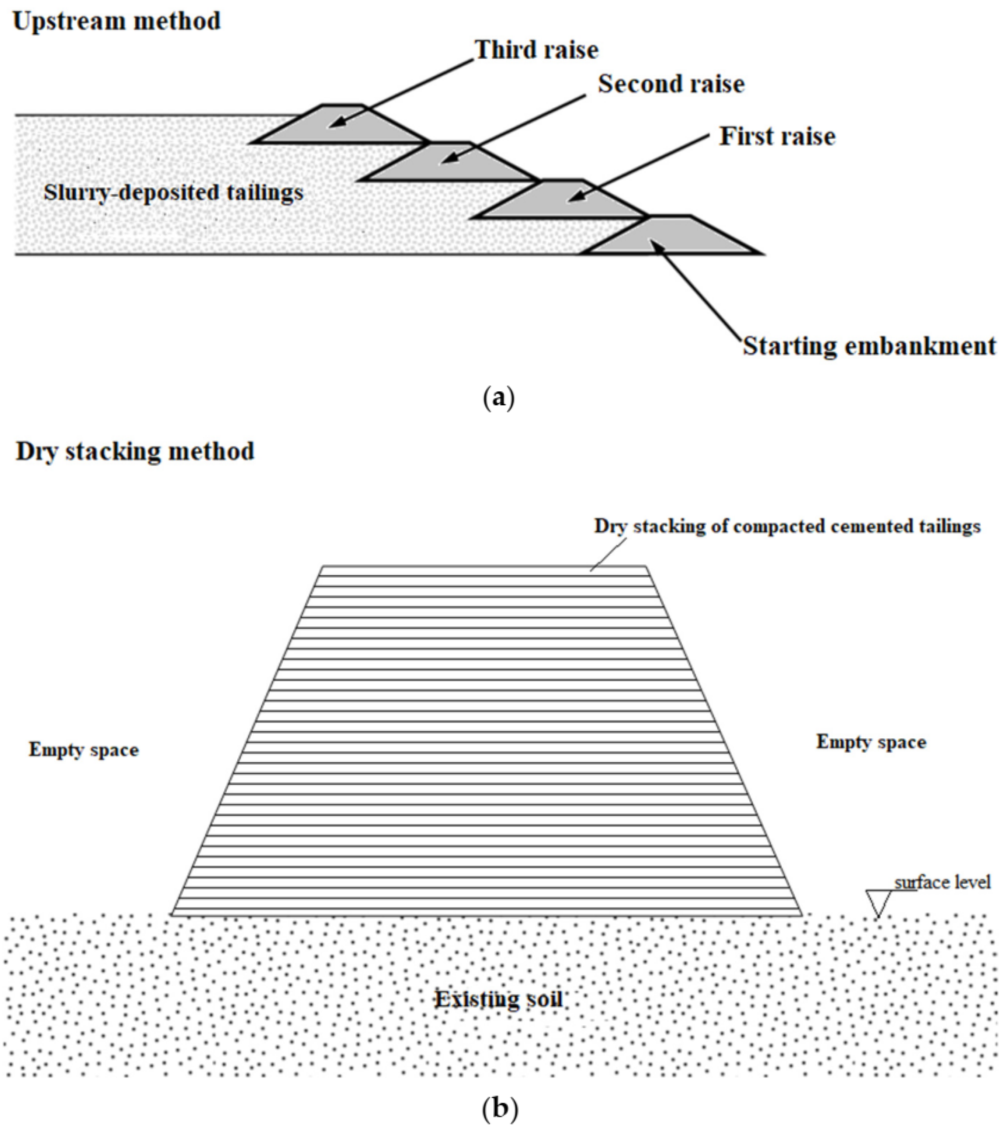

Figure 1. Schemes of tailings dam construction methods (**a**) upstream method (**b**) dry stacking method.

Dry stack tailings (Figure 1b) are being adopted in Brazil as a potential solution for reducing the risk of catastrophic dam failure and tailings runout. Essentially, they consist of the stacking of compacted dry tailings, forming piles of hundreds of meters. In this regard, the use of compacted filtered ore tailings–Portland cement blends stacking will allow tailings disposal sites, which currently do not use binders and thus have shallow slopes, to occupy smaller areas by creating steeper, more stable stacks which will consequently lead to less environmental and visual impact. The current research is studying the stress–strain–strength behaviour of artificially cemented (using Portland cement) compacted filtered iron mining tailings for stacking in order to drastically reduce the possibility of tailings liquefaction once cementitious bonds (cohesion) are built amongst tailings particles. The reason for studying especially iron mine tailings specifically is that Brazil is the second largest producer of iron ore (and consequently iron ore tailings) in the world, with approximately 388 million metric tons produced in 2020 [10].

Recognizing the topic's importance and based on concepts of ground improvement, this research aims to contribute to understanding the mechanical behaviour of compacted (considering distinct dry unit weights) iron ore tailings stabilized with early strength Portland cement (in distinct amounts), from unconfined compression, initial shear stiffness, performance under wetting–drying cycles and consolidated drained triaxial tests points of view.

2. Background

The characteristics of ore tailings are highly variable depending on the composition of the ores and the extraction processes used. In general, tailings can vary in size from colloidal to sand, with the degree of plasticity depending on the surface activity of the fines content [11]. The most common disposal method for tailings is hydraulic deposition, followed by sedimentation in an impoundment and consolidation under their own weight, which may take many years due to their relatively low hydraulic conductivity [12,13].

Frequently, the disposal conditions of relatively small size particles result in a saturated and low strength environment—often susceptible to liquefaction, caused by either static or seismic loading. In general, the large mudflows that follow dam failures imply the presence of loose, water-saturated sediments that want to contract upon shear. The water cannot drain fast enough, and grains become temporarily suspended, forming a dense fluid [9], which characterizes the liquefaction phenomenon. Conceptually, Jefferies and Been [14] define soil liquefaction as a phenomenon in which soil loses much of its strength or stiffness for a generally short time but nevertheless long enough to cause failures which result in large financial losses, environmental damage and, in the worst cases, loss of life. This is particularly important, since there are many incidents on tailings impoundments that are claimed to be related to liquefaction.

The stability performance of mine tailings is linked to their dry unit weight (γ_d) and consequently compaction could reduce liquefaction potential [15]. However, the existence of cementitious bonds amongst tailings particles (due to blends of tailings with Portland cement) prevents them of suffering liquefaction and enhances mechanical behaviour.

3. Experimental Program

3.1. Materials

The iron tailings used in the testing were taken from the Iron Quadrangle region, located in the province of Minas Gerais, Brazil (see Figure 2). The grain size distribution of the iron mine tailings is given in Figure 3. The iron mine tailings' physical properties are displayed in Table 1, being classified [16] as silty sand (SM). Mineralogical characterization of the iron tailings, acquired using an X-ray diffractometer, detected the presence of a few compounds: quartz [SiO_2], hematite [Fe_2O_3], goethite [$FeHO_2$], kaolinite [$Al_2H_4O_9Si_2$], and muscovite [$Al_3H_2KO_{12}Si_3$]. Regarding the chemical composition of the studied iron tailings, the following element concentrations were found after X-ray fluorescence: 69.7% of SiO_2, 24.0% of Fe_2O_3, 4.8% Al_2O_3, 0.40% of MnO, 0.25% of P_2O_5, 0.15% of K_2O, and 0.1% of SO_3, amongst others. The results of standard (600 kN.m/m^3) and modified (2700 kN.m/m^3) Proctor compaction tests are displayed in Figure 4.

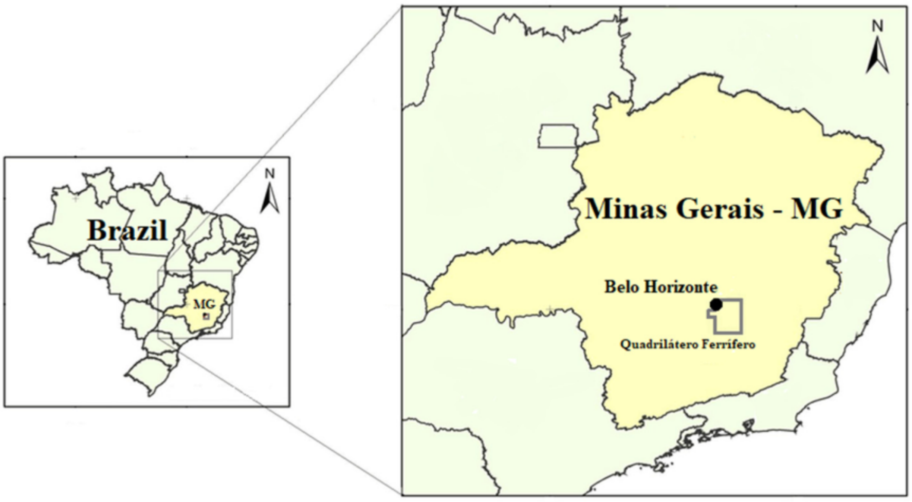

Figure 2. Location of the Iron Quadrilateral on the map of Brazil and Minas Gerais (MG) province.

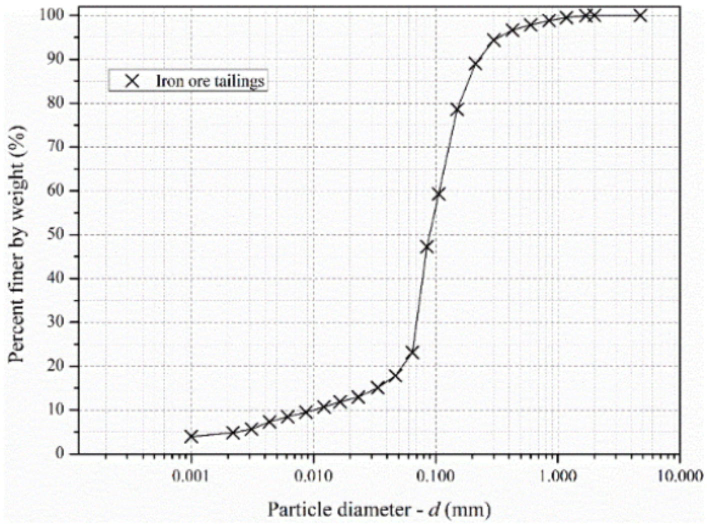

Figure 3. Iron ore tailings grain size distribution.

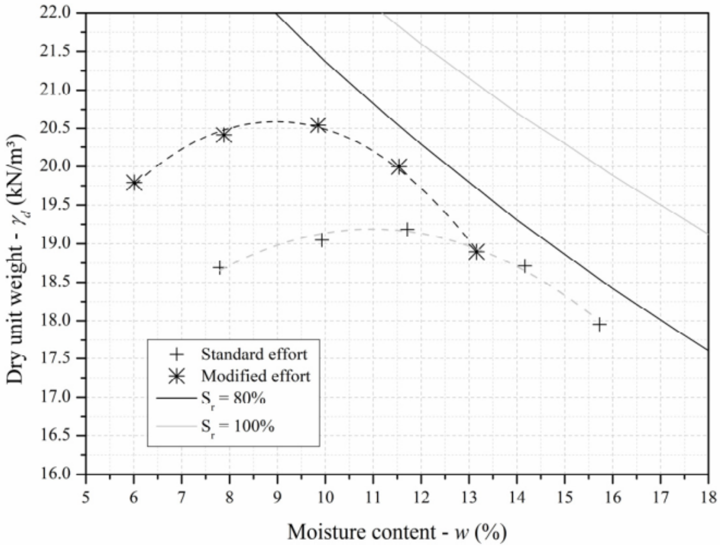

Figure 4. Compaction curves of iron ore tailings at standard and modified energies.

Table 1. Physical properties of studied iron ore tailings.

Physical Properties	Iron Ore Tailings (IOT)
Specific gravity of solids	2.916
Uniformity coefficient	10.7
Coefficient of curvature	3.9
Mean particle diameter-(mm)	0.085
Liquid limit (%)	-
Plastic limit (%)	-
Plasticity index (%)	Nonplastic
Medium sand (0.425 mm < d < 0.200 mm) (%)	4.0
Fine sand (0.075 mm < d < 0.425 mm) (%)	49.0
Silt (0.002 mm < d < 0.075 mm) (%)	42.0
Clay (d < 0.002 mm) (%)	5.0
USCS Classification (ASTM 2017)	SM
Maximum dry unit weight at standard energy compaction (kN/m^3)	19.2
Optimum moisture content at standard energy compaction (%)	11.6

High early strength (Type III) Portland cement [17] was used throughout this investigation. Its rapid strength gain allows blends to achieve important strength thresholds from short curing periods. Cement grains' specific gravity is 3.15.

Distilled water was utilized both for characterization tests and moulding specimens for the triaxial tests.

3.2. Methods

3.2.1. Moulding Portland Cement Stabilized Iron Ore Tailings (IOT) Specimens

Cylindrical specimens (50 mm in diameter and 100 mm in height) were moulded for the unconfined compression and initial shear stiffness tests, as well as for performance under wetting–drying and for consolidated isotropically drained triaxial tests using the undercompaction method [18]. A target dry unit weight (γ_d) for a particular specimen was then instituted as a result of the dry compacted iron tailings–Portland cement mix divided by the total volume of the specimen [19]. As exhibited in Equation (1) [20], porosity (η) is a function of dry density (γ_d) of the mix and Portland cement content (PC). Each substance (iron mine tailings and Portland cement) has a unit weight of solids (γs_{IOT} and γs_{PC}), which also must be measured for computing porosity.

$$\eta = 100 - 100\left\{\left[\frac{\gamma_d}{1+\frac{PC}{100}}\right]\left[\frac{1}{\gamma s_{IOT}} + \frac{\frac{PC}{100}}{\gamma s_{PC}}\right]\right\} \tag{1}$$

After the weighing of the dry materials (i.e., iron mine tailings and cement), these were manually mixed with a spoon until a powder having a visual uniformity was obtained. Next, the correct amount of distilled water was supplemented to reach moisture content of 11.6% (optimum moisture content for standard Proctor compaction effort—see Table 1) for the iron tailings—Portland cement blend, and the mixture continued up to the formation of a homogeneous paste. Following, the specimen was statically compacted inside a cylindrical split mould to its target dry unit weight. Three layers were used in the compaction process, with the top of the first and second layers being slightly scarified in order to guarantee the adherence of the subsequent layer. Once the moulding was finished, the specimen was retrieved from the mould, measured, weighed and sealed inside a plastic bag (to maintain water content) and sent to be cured in a humid room at 23 ± 2 °C with relative moisture of about 95%. As acceptance criteria, the obtained dry unit weight (γ_d) should range within ± 1% of the target value, whereas the moisture content (w) should be around 0.5% of the previously assigned value. Within each tested dosage, the cement content was calculated over the mass of dry iron mine tailings and the dry unit weight (γ_d) was determined as the ratio between the mass of dry solids and the total volume of the test specimen.

3.2.2. Program of Unconfined Compression Tests

The unconfined compression tests followed the ASTM C39 standard [21]. Specimens were moulded with 11.6% of moisture content (optimum moisture content for standard Proctor compaction effort), dry densities of 17 kN/m^3, 18 kN/m^3 and 19 kN/m^3 (corresponding to 89%, 94% and 99% of degree of compaction of standard Proctor compaction effort, respectively), Portland cement contents of 1%, 2%, 3%, 4% and 5% (determined following international [22] and Brazilian [23,24] experience with soil–cement). Specimens were cured for 2, 4, 7, 28 and 90 days. One day prior to the test, the specimens were submerged in a water container for 24 h in order to reduce possible suction effects [20,23]. The temperature of the water tank was controlled according to the adopted curing temperature (i.e., 23 °C). Next, the unconfined compression test was performed using an automatic loading press with maximum capacity of 50 kN at a displacement rate of 1.14 mm/min; the maximum load measured using a load cell. A full factorial design setting was used to define the mix designs for the tests. For this reason, all possible combinations of amounts of cement and dry unit weight values were tested considering each curing period. Thus, 15 dosages were intended to be tested within each curing time; in triplicate moulded for each dosage.

3.2.3. Program of Pulse Velocity Tests and Ultrasonic Elastic Constants

Initial Shear Modulus (G_0) of artificially cemented soils can be determined using ultrasonic pulse velocity tests performed in accordance with ASTM D2845 [25]. For homogeneous and elastic media, G_0 may be calculated through the product between the bulk density and the square of the velocity of a shear wave passing through it [26]. Therefore, as this test is non-destructive, pulse velocity tests were performed on the same specimens moulded for an unconfined compression test, immediately before taking specimens to failure, using special transducers coupled on top and underneath the samples using a special coupler gel. An ultrasonic pulse device was used to emit compression (54 kHz) and shear waves (250 kHz) that are emitted and cross the cylindrical specimens, with the propagation times measured. Therefore, the shear modulus at very small deformations (G_0) can be obtained.

3.2.4. Program of Durability of Specimens Submitted to Wetting–drying Cycles

Durability tests consisting of wetting–drying cycles were carried out in accordance with ASTM D559 [27], but without brushing. Specimens were moulded with 11.6% of moisture content, dry densities of 17 kN/m^3, 18 kN/m^3 and 19 kN/m^3, and Portland cement contents of 1%, 2%, 3%, 4% and 5%. The same experimental design setting previously described for the strength tests was used herein, with the difference that only one specimen for each dosage was tested. This test method aims to simulate harsh on-field conditions over 12 cycles of such procedures [28]. After 2, 4, and 7-days of curing were completed, each specimen cycle started by immersing it in water for 5 h at 23 °C. Then, specimens were submitted to a drying process in an oven during 42h at 71 °C. Twelve cycles of these procedures are required to simulate harsh on-field conditions. After each one of the 12 cycles, the initial shear modulus (G_0) was measured in accordance with ASTM D2845 [25]. After the 12th cycle, specimens were taken to failure through unconfined compression tests in accordance with the ASTM C39 standard [21].

3.2.5. Program of Consolidated Isotropically Drained (CID) Triaxial Tests

A series of consolidated isotropically drained (CID) triaxial compression tests was conducted on artificially cemented compacted filtered iron mining tailings, with the aim of evaluating the deviatoric stress–axial strain–volumetric strain behaviour of the materials. The general procedures described by BS 1377 were followed [29]. In this regard, two representative dosages were chosen and tested under three effective confining pressures (σ'_3 = 50, 100 and 200 kPa). The first dosage contained 3% of cement and was moulded at a dry unit weight of 17 kN/m^3, and the second had the same amount of cement but was compacted to a dry density of 19 kN/m^3. The pressures throughout the tests were electronically monitored by pressure transducers, whereas the vertical load was assessed using a 20 kN high-resolution load cell. The axial displacements were globally measured using a linear variable differential transformer (LVDT) and locally assessed by Hall effect sensors positioned directly in contact with the test specimen [30]. The volumetric strain was measured by an Imperial College volume gauge [31] connected to the drainage outlet. To ensure the saturation of tailings specimens, a back pressure of approximately 500 kPa was applied to produce B parameters higher than 95%. All reported test specimens were isotropically consolidated to their desired consolidation pressure before shearing. Finally, shearing of specimens in triaxial tests occurred at a rate of 1 mm/h. For the calculation of the applied stresses, the area corrections proposed by La Rochelle et al. [32] were adopted.

4. Results and Analysis

4.1. Unconfined Compressive Strength (q_u)

Figure 5a portrays q_u as a function of porosity/cement index (η/C_{iv}) (stated as porosity (η) divided by the volumetric cement content (C_{iv}), the latter expressed as a percentage of cement volume to the total volume of the iron tailings–Portland cement mixes [33]) for the curing periods studied (2, 4, 7, 28 and 90 days). Diambra et al. [34] carried out the theoretical approach validating the shape of the equation. Figure 5a indicates that the η/C_{iv} index is useful in normalizing strength results for iron ore tailings–Portland cement blends. The results indicate that the behaviour of the studied blends presents the same trend, thus generating a single equation (Equation (2)).

$$q_u(\mathrm{kPa}) = A \times 10^4 \times \left[\frac{\eta}{C_{iv}}\right]^{-D} \tag{2}$$

Scalar "D" has been found to be a constant (D = 1.3) to all curing times studied (from 2 to 90 days), while scalar "A" increases with curing time, as shown in Table 2. "A" changes from 1.63 (for 2 days of curing) to 4.89 (for 90 days of curing) and the coefficient of determination (R^2) varies in the range 0.92 to 0.97. From 2 days of curing to 4, 7, 28 and 90 days of curing, the strength increase percentages were of 63.2%, 82.8%, 147.9% and 200.0%, respectively.

Table 2. "A" and "C" scalars for Equations (2) and (3), respectively.

Curing Period	Strength Data—q_u		Stiffness Data—G_0	
	"A"	Coefficient of Determination (R^2)	"C"	Coefficient of Determination (R^2)
2 days	1.63	0.92	1.46	0.86
4 days	2.66	0.96	2.98	0.92
7 days	2.98	0.97	4.11	0.97
28 days	4.04	0.94	4.53	0.96
90 days	4.89	0.96	6.04	0.96

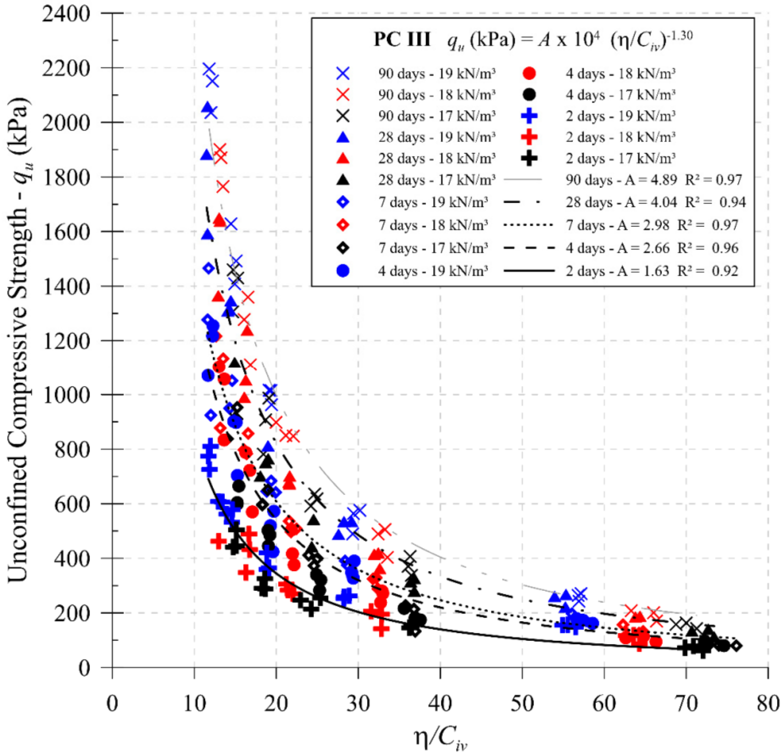

(**a**)

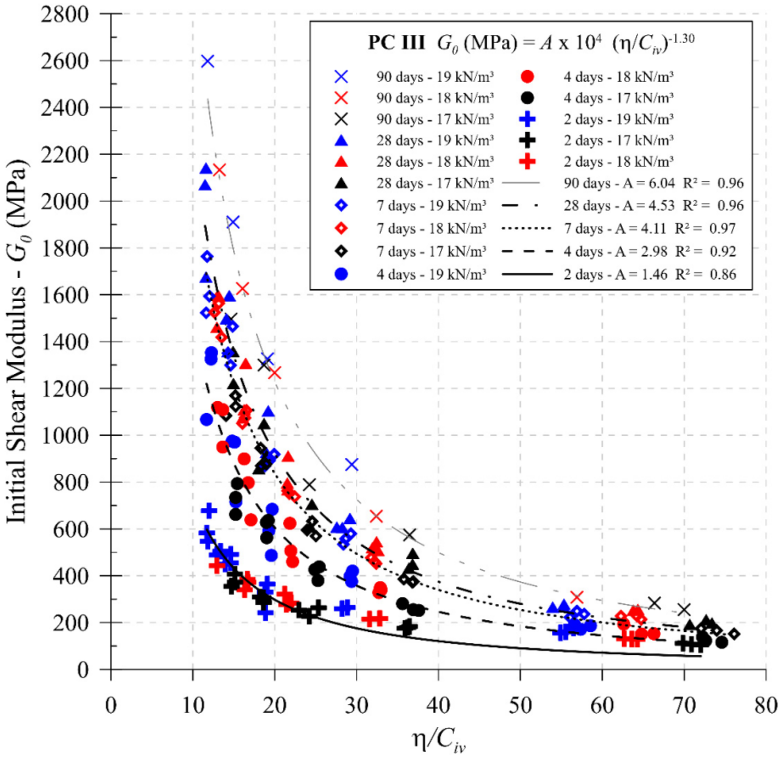

(**b**)

Figure 5. Compacted (γ_d = 17 kN/m^3, γ_d = 18 kN/m^3, γ_d = 19 kN/m^3) filtered iron mining tailings treated with early strength Portland cement (from 1% to 5%): (**a**) unconfined compressive strength (q_u) versus porosity/cement index (η/C_{iv}) considering distinct curing time periods and (**b**) initial shear stiffness (G_0) versus η/C_{iv} taking under consideration different curing time periods (2, 4, 7, 28 and 90 days of curing).

4.2. Initial Shear Modulus

Similarly, as presented for the unconfined compressive strength test results, the porosity/cement index was used for the initial shear modulus (G_0) results for the curing periods studied (2, 4, 7, 28 and 90 days), as presented in Figure 5b. Therefore, an adequate association between G_0 and the η/C_{iv} index (considering the same power shape as for strength) could be obtained as the coefficient of determination (R^2) varies in the range 0.86 to 0.97 for the studied curing times, in the format of a specific equation (Equation (3)).

$$G_0(\text{MPa}) = C \times 10^4 \times \left[\frac{\eta}{C_{iv}}\right]^{-E} \quad (3)$$

Scalar "E" has been found to be a constant (E = 1.3) for all curing times studied (from 2 to 90 days), while scalar "C" increases with curing time, as shown in Table 2. "C" changes from 1.46 (for 2 days of curing) to 6.04 (for 90 days of curing). From 2 days of curing to 4, 7, 28 and 90 days of curing, the initial shear modulus (G_0) increase percentage were of 104.1%, 181.5%, 210.3% and 313.7%, respectively. It is interesting to observe that the rate of increase of q_u and G_0 was not the same with curing time. The rate of increase of G_0 was higher up to 28 days of curing and the rate of increase of q_u was higher from 28 days to 90 days of curing.

4.3. Durability under Wetting–Drying Cycles

Figure 6 presents G_0 variation of iron ore tailings compacted at γ_d of 17, 18 and 19 kN/m^3 and treated with 1 to 5% of early strength Portland cement. Wetting–drying cycles were performed after 2, 4 and 7 days of curing. Such performance mimics the behaviour of the studied blends after being submitted to harsh on-field conditions over 12 cycles of such procedures. It is well established that increasing both the quantity of cement and γ_d improves the stiffness of the compacted iron ore tailings–Portland cement mixes considering wetting–drying cycles. Disregarding the initial curing time (2, 4 or 7 days), Figure 6 shows a comparable qualitative response regarding the impact of wetting–drying cycles: G_0 increased from zero to three wetting–drying cycles and then oscillated about an average, distinctive for each γ_d and quantity of cement employed, for additional cycles. The oven drying for 42 h at 71 ± 2 °C, during the drying part of the wetting–drying cycles, triggered the catalysis of the chemical reactions of the Portland cement, bringing about the increase of G_0 of iron tailings–Portland cement mixes in the initial cycles. Distinct results were achieved by Consoli et al. [28], who assessed the effect of wetting–drying cycles on G_0 of a nonplastic silt. Test results by Consoli et al. [28] indicated that G_0 of nonplastic silt–Portland cement (also early strength) blends mostly reduced with more wetting–drying cycles, reaching a steadiness at about six wetting–drying cycles.

Figure 7 presents the correlation of q_u and G_0 as a function of η/C_{iv} index after 12 wetting–drying cycles. Looking at q_u results Figure 7a, it can be noticed that after 12 wetting–drying cycles, q_u is related to η/C_{iv} index through Equation (4). This equation has the same form as Equation (2) and the scalar of present equation is found above results of 90 days of curing at 23 °C. The q_u, after 12 wetting–drying cycles, being above the results of 90 days of curing at 23 °C is an example of enhancement triggered by the catalysis of the chemical reactions of the Portland cement, due to oven drying for 42 h at 71 ± 2 °C.

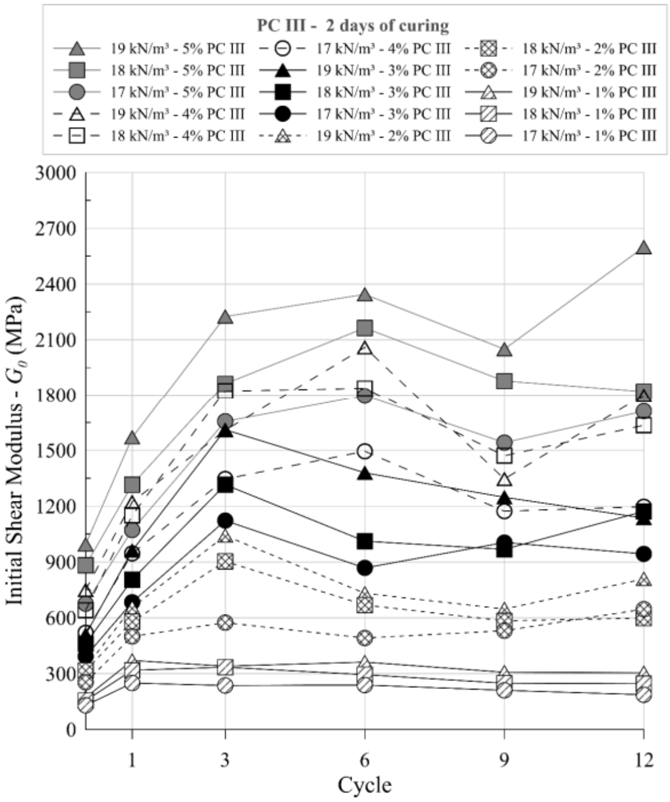

(**a**)

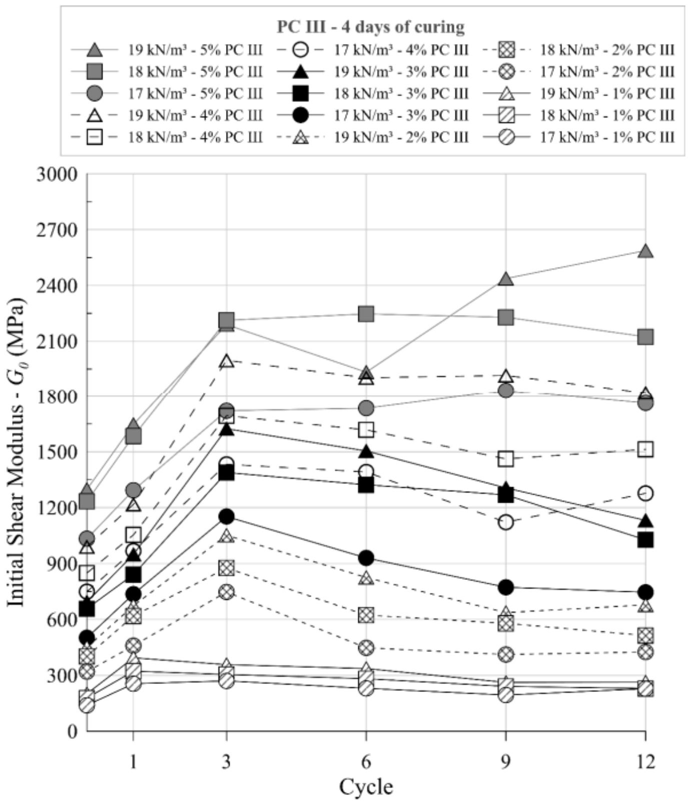

(**b**)

Figure 6. *Cont.*

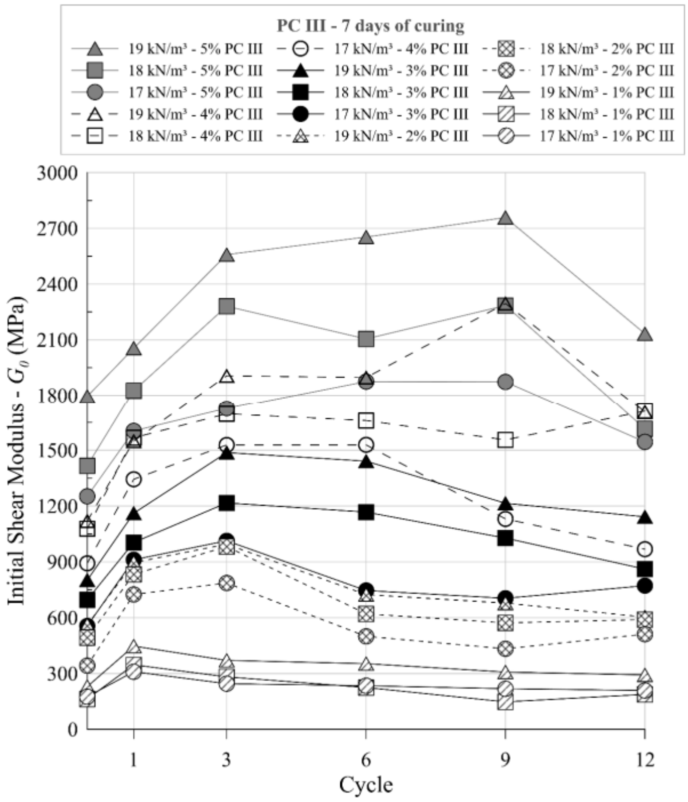

(**c**)

Figure 6. Performance (initial shear stiffness (G_0) variation) of compacted iron ore tailings treated early strength Portland cement after wet–dry cycles after: (**a**) curing for 2 days, (**b**) curing for 4 days and (**c**) curing for 7 days.

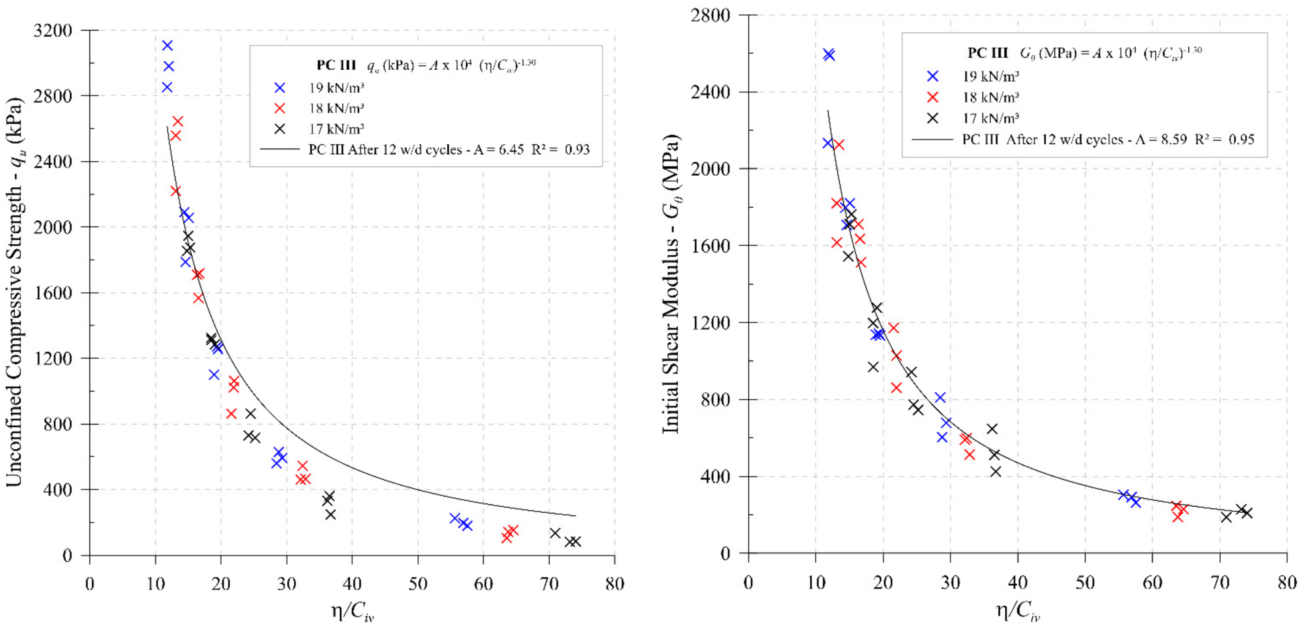

(**a**) (**b**)

Figure 7. Compacted filtered iron mining tailings treated with early strength Portland cement and cured for 2, 4 and 7 days: (**a**) q_u versus η/C_{iv} after 12 wet-dry cycles and (**b**) G_0 versus η/C_{iv} after 12 wetting–drying cycles.

On the other hand, focusing on the G_0 results in Figure 7b, it can be noted that after 12 wetting–drying cycles, G_0 is related to η/C_{iv} index through Equation (5). Such an equation has the same form as Equation (3), and the scalar of present equation is higher than the results of 90 days of curing at 23 °C. However, for q_u and G_0, results after 12 wetting–drying cycles are of the same order of magnitude as the results after 90 days of curing at 23 °C.

$$q_u(\text{kPa}) = 6.45 \times 10^4 \times \left[\frac{\eta}{C_{iv}}\right]^{-1.30} \tag{4}$$

$$G_0(\text{MPa}) = 8.59 \times 10^4 \times \left[\frac{\eta}{C_{iv}}\right]^{-1.30} \tag{5}$$

4.4. Triaxial

Figure 8 presents the stress–axial strain–volumetric strain curves of the standard consolidated drained triaxial tests of artificially cemented specimens of iron ore tailings moulded with γ_d of 17 kN/m^3 and 19 kN/m^3. All specimens have shown a quite stiff response at small axial strains (connected to the contraction of the material), followed by quite brittle behaviour (strong strain-softening response), and the tendency to dilation of the material. The brittleness and dilation tendency are gradually suppressed due to the increase of confining pressures.

The peak failure envelope leads to a peak angle of shearing resistance (φ'_{peak}) of about 34.1° for both dry unit weights and a peak cohesion intercept of (c'_{peak}) of 80.9 kPa for (γ_d) of 17 kN/m^3 and 157.2 kPa for (γ_d) of 19 kN/m^3. The increase of the degree of compaction at standard Proctor energy from 89% to 99% did not cause any change in φ'_{peak} but almost double c'_{peak}. On the other side, the critical state line reaches an angle of shearing resistance at a critical state (φ'_{cs}) of 36.3°.

Values of secant deformation modulus (E_{sec}), obtained at axial strains of 0.1%, 0.5% and 1.0% and for confining stresses ranging from 50 to 200 kPa, are presented in Table 3. Regarding the specimens prepared with γ_d = 17 kN/m^2, it can be seen in Table 3 that the higher modulus is E_{sec} = 816.1 MPa (for ε_a = 0.1% and confining pressure of 200 kPa), while for specimens prepared with γ_d = 19 kN/m^3, the higher modulus is E_{sec} = 2599.9 MPa; the latter (γ_d = 19 kN/m^2) being more than three times the secant modulus value at γ_d = 17 kN/m^3.

Table 3. Secant modulus (E_{sec}) of cement treated iron ore tailings (at distinct axial strains) considering dry unit weights of (a) γ_d = 17 kN/m^3 and (b) γ_d = 19 kN/m^3.

γ_d = 17 kN/m^3 & 3% PC III				**γ_d = 19 kN/m^3 & 3% PC III**			
		E_{sec} (MPa)				**E_{sec} (MPa)**	
Confining Pressure	ε_a (%) = 0.1	ε_a (%) = 0.5	ε_a (%) = 1.0	Confining Pressure	ε_a (%) = 0.1	ε_a (%) = 0.5	ε_a (%) = 1.0
50 kPa	714.7	441.6	355.1	50 kPa	1888.9	1412.8	378.6
100 kPa	740.2	605.3	524.2	100 kPa	2042.7	1652.9	812.5
200 kPa	816.1	500.1	526.6	200 kPa	2599.9	1808.6	965.3
(a)				(b)			

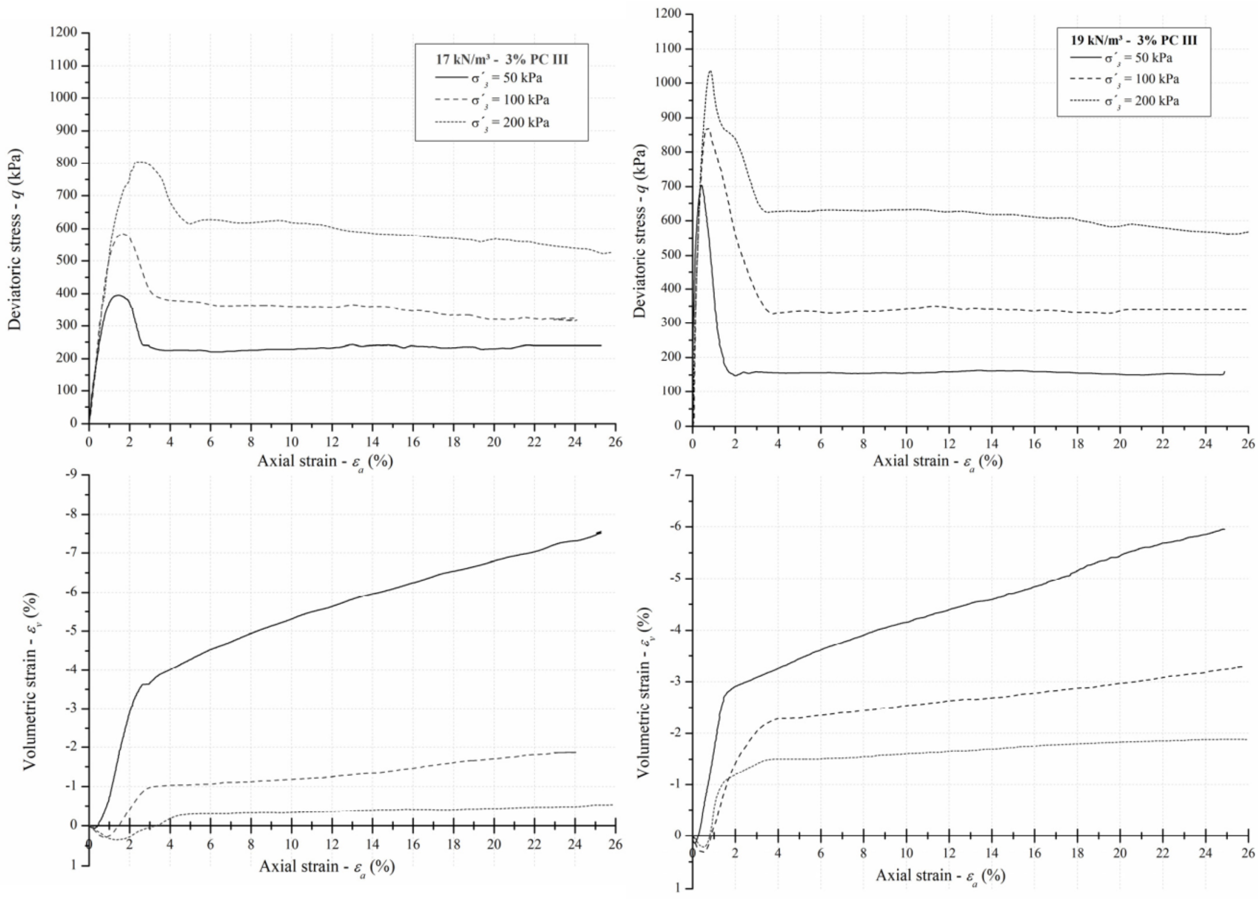

(**a**) (**b**)

Figure 8. Stress–axial strain–volumetric strain curves for the consolidated drained triaxial tests of specimens moulded with (**a**) γ_d of 17 kN/m^3 and 3% of early strength Portland cement blended with iron tailings under confining pressures of 50, 100 and 200 kN/m^3 and (**b**) γ_d of 19 kN/m^3 and 3% of early strength Portland cement blended with iron tailings under confining pressures of 50, 100 and 200 kN/m^3.

5. Discussion

An original study with the objective of contributing to the understanding of the geomechanical behaviour of a new form of iron ore tailings disposal (stacking of compacted filtered ore tailings–Portland cement blends) was presented as an alternative method to the conventional tailings dam disposal. Adequate correlations between the η/C_{iv} index with q_u and G_0 through power functions were obtained (Figure 5). In artificially cemented soils the η/C_{iv} ratio is usually adjusted by a power (ξ) applied to the variable C_{iv} (defined by curve fitting) to make the rates of variation of η and $1/C_{iv}$ compatible [20]. The value of ξ determines the greater or lesser contribution of porosity or cement content in the mechanical response. According to Diambra et al. [34], its magnitude is directly associated with the properties of the soil matrix and usually approximates the inverse of the exponent of the power function ($\xi \approx 1/D$ or $1/E$ in Equations (2) and (3), respectively). In the present study, an assumed value of ξ = 1 allowed the best fit ($R^2 > 0.92$) for correlating the η/C_{iv} index with q_u, G_0 and durability.

Rios et al. [35], working with a residual soil of very low (or no) plasticity corresponding to a well graded silty sand and with three different grain size fractions of this same soil determined that, under conditions of similar mineralogy, the particle size distribution is the most relevant factor in the definition of the magnitude of ξ. The research concludes that soils with higher fines (silt) content, fine sand fraction, and better graded, with broader grain size distribution curves, reported lower power values ($\xi \approx 0.21$) compared to poorly graded and fine to coarse sandy soil fractions ($\xi \approx 1$). However, mineralogical composition (related to particle shape) is reported as the most decisive factor in the magnitude of ξ, reporting adjusted values of ξ = 1 and ξ = 0.1 when comparing two uniform sands (with similar particle size distribution) characterized by having majority quartz and mica phases, respectively. The preponderant contents of quartz and iron minerals (hematite and goethite) in the filtered iron ore tailings determine the value of the fitting power (ξ = 1). Values of ξ = 1 have been widely reported in the literature for the definition of dosage equations in soils of granular or frictional nature treated with Portland cement [36]. This value, equal to unity, determines an equivalent influence between porosity and cement volumetric content on q_u, G_0 and durability.

Adding cement is considered an effective procedure to prevent liquefaction of soils. In general, the behaviour pattern of filtered iron ore tailings–Portland cement blends is determined by brittle and strain softening behaviour at low confining stresses (mainly due to cementing agent bonds), which evolves to more gentle strain softening with peak strength occurring at higher axial strains as confining stress levels increase (Figure 8). This behaviour is analogous to that reported for a wide range of cemented sands tested at low confining stresses [37,38]. The larger the γ_d of the compacted specimens (lower η), the larger the peak deviator stress reached, the stiffer and more dilative the material, and the greater the post-peak drop in the deviator stress. On the other hand, volumetric strains are strongly dilatant at low stress levels. Some authors (e.g., Airey [39], Coop and Willson [40], Consoli et al. [38]), from the study of different artificially and naturally cemented sands, agree that at high confining stresses (higher than those investigated here) volumetric strains tend towards compression. Additionally, a cohesive behaviour (dominated by cement) at low confining stresses and/or high cement contents tends to evolve to a frictional behaviour (dominated by the sand matrix) at high confining stresses and/or low cement contents.

Figure 9 shows the deviatoric stress—axial strain—volumetric strain curves (for consolidated drained triaxial tests) of the uncemented filtered iron ore tailings and 3% early strength Portland cement mixed with the iron ore tailings, both compacted to a γ_d of 17 kN/m^3 and submitted to confining stresses of 200 kPa. The uncemented filtered iron ore tailings show strong contractive behaviour, confirming the relevance of compressibility of the filtered iron ore tailings and the possibility of uncontrolled positive pore-pressure generation if under undrained shear conditions, which would lead to loss of effective stresses and increased liquefaction potential of the tailings at relatively low confining stresses. In contrast, the occurrence of volumetric dilatational strains (generation of negative pore-pressures if under undrained shear conditions), at low stress levels, and high peak cohesion intercepts (c'_{peak}) reported in tailings treated with the addition of 3% cement would reduce the liquefaction potential of compacted filtered iron ore tailings piles.

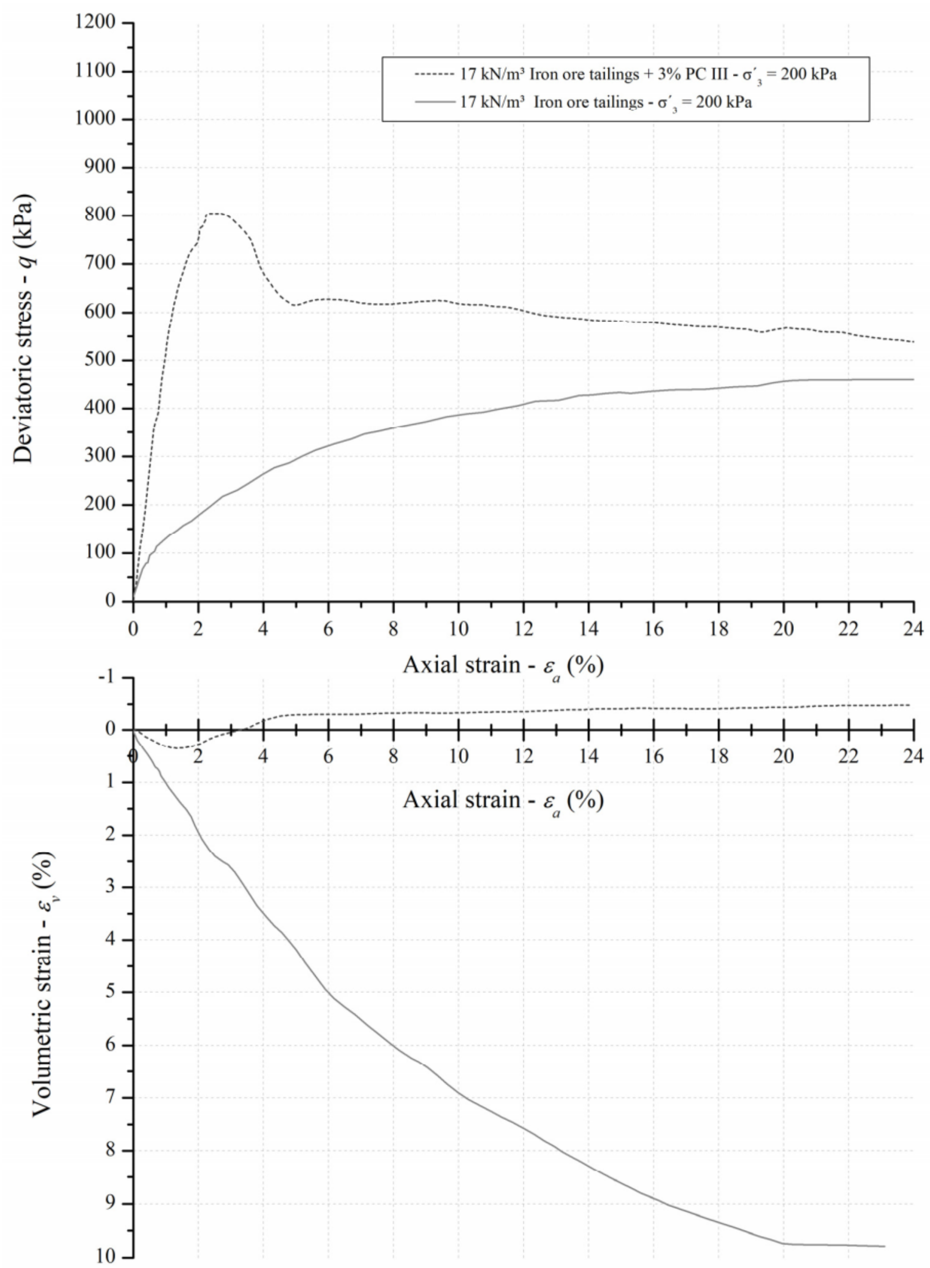

Figure 9. Stress–axial strain–volumetric strain curves for the consolidated drained triaxial tests of specimens moulded with filtered iron ore tailings and 3% early strength Portland cement mixed with iron ore tailings at a dry unit weight (γ_d) of 17 kN/m^3 under confining pressures of 200 kN/m^3.

6. Conclusions

An extensive laboratory testing program was carried out to investigate the effectiveness of using Portland cement and compaction energies to evaluate the engineering behaviour of filtered iron ore tailings. The observations and conclusions can be summarized as follows:

The employment of the porosity/cement index (η/C_{iv}) with the purpose of expressing the performance of iron ore tailings combined with the incorporation of Portland cement and densification through compaction, with curing periods varying from 2 to 90 days, can be considered successful. High coefficients of determination were obtained when q_u and G_0 results were correlated with this parameter. Based on the dosage equations established in present research for the studied iron ore tailings–Portland cement blends, there are several technical ways of reaching a q_u or a G_0 target value for a given project and the best solution might change from situation to situation depending on the time period available for curing, accessibility to equipment to reach a given porosity and cost of Portland cement.

The stress–strain response showed a strength peak for all the samples and a softening following a peak. Also, the increase in effective stress causes an expansive response in volumetric strain. The peak failure envelope leads to a peak angle of shearing resistance (φ'_{peak}) of about 34.1° for both dry unit weights and a peak cohesion intercept of (c'_{peak}) of 80.9-kPa for (γ_d) of 17-kN/m^3 and 157.2-kPa for (γ_d) of 19-kN/m^3. The increase of the degree of compaction at standard Proctor energy from 89% to 99% did not cause any change in φ'_{peak} but almost double c'_{peak}. On the other side, the critical state line reaches an angle of shearing resistance at critical state (φ'_{cs}) of 36.3°. The use of 3% of Portland cement for triaxial testing represents an intermediate amount of cement studied in this research.

The present work has been envisaged as a contribution to the behaviour of compacted iron ore tailings–Portland cement blends to be disposed by stacking. The influence of degree of compaction as well as the amount of Portland cement on strength and stiffness properties was evaluated. The blends studied herein were compacted at optimum moisture content. It might not be possible to do so in the field, especially during rainy seasons. Therefore, the influence of compaction moisture content in the mechanical behaviour requires further study. Another point requiring future research is the development of alternative sustainable binders for stabilization of stacking filtered tailings in order to have a less costly, greener engineering solution. It is also necessary to emphasize that the present study was constrained to the range of low to medium confining pressures, making it attractive to tailings disposal by stacking up to heights of 10–12 m. Other studies are necessary to evaluate changes in the behaviour of the material under higher stackings, when the confining pressure will be greater than the studied range. At last, the addition of a binder to the compacted filtered tailings reduces the volume of hydraulically carried out sediments, thus allowing smaller sedimentation structures downstream of the disposal structure (e.g., ponds and sedimentation dikes).

Author Contributions: Conceptualization, N.C.C.; methodology, N.C.C. and A.L.; validation, N.C.C., H.M.C. and E.B.M.; formal analysis, N.C.C. and H.C.S.F.; investigation, A.L., H.M.C. and E.B.M.; resources, N.C.C.; data curation, N.C.C., H.C.S.F. and E.B.M.; writing—original draft preparation, N.C.C.; writing—review and editing, N.C.C., J.C.V., J.P.S.S. and A.L.; supervision, N.C.C.; project administration, N.C.C.; funding acquisition, N.C.C. All authors have read and agreed to the published version of the manuscript.

Funding: The authors wish to make explicit their appreciation to VALE S.A. (IAP-001247 and IAP-001466) and CNPq (Brazilian Research Council) for the support to the research group.

Institutional Review Board Statement: Not applicable.

Informed Consent Statement: Not applicable.

Data Availability Statement: Some or all data, or models, used during the study are available from the corresponding author upon reasonable request.

Conflicts of Interest: The authors declare no conflict of interest. The funders had no role in the design of the study; in the collection, analyses, or interpretation of data; or in the decision to publish the results.

Abbreviations

A, C, D, E	scalars
B	Skempton's parameter
c'_{peak}	peak cohesion at effective stresses
C_{iv}	volumetric cement content
d	particle diameter
E_{sec}	secant modulus
G_0	initial shear modulus

IOT	iron ore tailings
PC	Portland cement
q_u	unconfined compressive strength
ξ	power function parameter
ε_a	axial strain
ε_v	volumetric strain
γ_d	dry unit weight
γ_s	unit weight of solids
φ'_{cs}	angle of shearing resistance at critical state
φ'_{peak}	peak angle of shearing resistance at effective stresses
η	porosity
η/C_{iv}	porosity/cement index

References

1. Li, W.; Coop, M.; Senetakis, K.; Schnaid, F. The mechanics of a silt-sized gold tailing. *Eng. Geol.* **2018**, *241*, 97–108. [CrossRef]
2. Kossoff, D.; Dubbin, W.; Alfredsson, M.; Edwards, S.; Macklin, M.; Hudson-Edwards, K. Mine tailings dams: Characteristics, failure, environmental impacts, and remediation. *Appl. Geochem.* **2014**, *51*, 229–245. [CrossRef]
3. Armstrong, M.; Langrené, N.; Petter, R.; Chen, W.; Petter, C. Accounting for tailings dam failures in the valuation of mining projects. *Resour. Policy* **2019**, *63*, 101461. [CrossRef]
4. Hu, L.; Wu, H.; Zhang, L.; Zhang, P.; Wen, Q. Geotechnical properties of mine tailings. *J. Mater. Civ. Eng.* **2017**, *29*, 04016220. [CrossRef]
5. World Mine Tailings Failures. State of World Mine Tailings Portfolio 2020. WMTF. 2020. Available online: https://worldminetailingsfailures.org/ (accessed on 15 November 2021).
6. United Nations Environment Programme. New Report Urges Global Action on Mining Pollution. UNEP. 2017. Available online: https://www.unep.org/news-and-stories/story/new-report-urges-global-action-mining-pollution (accessed on 15 November 2021).
7. Islam, K.; Murakami, S. Global-scale impact analysis of mine tailings dam failures: 1915–2020. *Glob. Environ. Chang.* **2021**, *70*, 102361. [CrossRef]
8. Lyu, Z.; Chai, J.; Xu, Z.; Qin, Y.; Cao, J. A comprehensive review on reasons for tailings dam failures based on case history. *Adv. Civ. Eng.* **2019**, *2019*, 4159306. [CrossRef]
9. Santamarina, J.C.; Torres-Cruz, L.A.; Bachus, R.C. Why coal ash and tailings dam disasters occur. *Science* **2019**, *364*, 526–528. [CrossRef] [PubMed]
10. Statista. Iron Ore Mine Production in Brazil from 2015 to 2020. Statista. 2021. Available online: https://www.statista.com/statistics/1026351/brazil-iron-ore-mine-production/ (accessed on 15 November 2021).
11. Vick, S.G. *Planning, Design, and Analysis of Tailings Dams*; Bitech: Vancouver, BC, Canada, 1990.
12. Consoli, N.C.; Sills, G.C. Soil formation from tailings: Comparison of predictions and field measurements. *Géotechnique* **2000**, *50*, 25–33. [CrossRef]
13. James, M.; Aubertin, M.; Wijewickreme, D.; Wilson, G.W. A laboratory investigation on the dynamic properties of tailings. *Can. Geotechnical J.* **2011**, *48*, 1587–1600. [CrossRef]
14. Jefferies, M.G.; Been, K. *Soil liquefaction: A critical state approach*; CRC Press: Boca Raton, FL, USA, 2015.
15. Villavicencio, G.; Breul, P.; Bacconnet, C.; Fourie, A.; Espinace, R. Liquefaction potential of sand tailings dams evaluated using probabilistic interpretation of estimated in-situ relative density. *Rev. De La Construcción* **2016**, *15*, 9–18. [CrossRef]
16. *ASTM D2487*; Standard practice for classification of soils for engineering purposes (Unified Soil Classification System); American Society for Testing and Materials: West Conshohocken, PA, USA, 2017.
17. *ASTM C150*; Standard specification for Portland cement; ASTM International: West Conshohocken, PA, USA, 2017.
18. Selig, E.; Ladd, R.S. Preparing test specimens using undercompaction. *Geotechnical Test. J.* **1978**, *1*, 16. [CrossRef]
19. *ASTM D7263*; Standard test methods for laboratory determination of density and unit weight of soil specimens; American Society for Testing and Materials: West Conshohocken, PA, USA, 2021.
20. Consoli, N.C.; da Fonseca, A.V.; Cruz, R.; Rios, S. Voids/cement ratio controlling tensile strength of cement treated soils. *J. Geotechnical Geoenvironmental Eng.* **2011**, *137*, 1126–1131. [CrossRef]
21. *ASTM C39*; Standard test method for compressive strength of cylindrical concrete specimens; American Society of Civil Engineers: West Conshohocken, PA, USA, 2018.
22. Mitchell, J.K. Soil improvement—State-of-the-art report. In Proceedings of the 10th International Conference on Soil Mechanics and Foundation Engineering, International Society of Soil Mechanics and Foundation Engineering, Stockholm, Sweden, 15–19 June 1981; pp. 509–565.
23. Consoli, N.C.; Foppa, D.; Festugato, L.; Heineck, K.S. Key parameters for strength control of artificially cemented soils. *J. Geotechnical Geoenvironmental Eng.* **2007**, *133*, 197–205. [CrossRef]
24. Consoli, N.C.; Ferreira, P.; Tang, C.-S.; Marques, S.F.V.; Festugato, L.; Corte, M.B. A unique relationship determining strength of silty/clayey soils–Portland cement mixes. *Soils Found.* **2016**, *56*, 1082–1088. [CrossRef]

25. *ASTM D2845*; Standard test method for laboratory determination of pulse velocities and ultrasonic elastic constants of rock; American Society for Testing and Materials: West Conshohocken, PA, USA, 2008.
26. Mitchell, J.K.; Soga, K. *Fundamentals of Soil Behavior*, 3rd ed.; John Wiley & Sons: Hoboken, NJ, USA, 2005.
27. *ASTM D559*; Standard test methods for wetting and drying compacted soil-cement mixtures; American Society for Testing and Materials: West Conshohocken, PA, USA, 2015.
28. Consoli, N.C.; Samaniego, R.A.Q.; González, L.E.; Bittar, E.J.; Cuisinier, O. Impact of severe climate conditions on loss of mass, strength, and stiffness of compacted fine-grained soils–Portland cement blends. *J. Mater. Civ. Eng.* **2018**, *30*, 04018174. [CrossRef]
29. *BS 1377*; Methods of test for soils for civil engineering purposes; British Standards: London, UK, 1990.
30. Clayton, C.R.I.; Khatrush, S.A. A new device for measuring local axial strains on triaxial specimens. *Géotechnique* **1986**, *36*, 593–597. [CrossRef]
31. Maswoswe, J.J. Stress Path Method for a Compacted Soil during Collapse Due to Wetting. Ph.D. Thesis, University of London, London, UK, 1985.
32. La Rochelle, P.; Leroueil, S.; Trak, B.; Blais-Leroux, L.; Tavenas, F. Observational approach to membrane and area corrections in triaxial tests. In Proceedings of the Advanced Triaxial Testing of Soil and Rock, Louisville, KY, USA, 19–20 June 1986; p. 715, (published by ASTM STP 977–1988).
33. Consoli, N.C.; Morales, D.P.; Saldanha, R.B. A new approach for stabilization of lateritic soil with Portland cement and sand: Strength and durability. *Acta Geotechnica* **2021**, *16*, 1473–1486. [CrossRef]
34. Diambra, A.; Ibraim, E.; Peccin, A.; Consoli, N.C.; Festugato, L. Theoretical derivation of artificially cemented granular soil strength. *J. Geotech. Geoenvironmental Eng.* **2017**, *143*, 04017003. [CrossRef]
35. Rios, S.; da Fonseca, A.V.; Consoli, N.C.; Floss, M.; Cristelo, N. Influence of grain size and mineralogy on the porosity/cement ratio. *Géotechnique Lett.* **2013**, *3*, 130–136. [CrossRef]
36. Diambra, A.; Festugato, L.; Ibraim, E.; da Silva, A.P.; Consoli, N.C. Modelling tensile/compressive strength ratio of artificially cemented clean sand. *Soils Found.* **2018**, *58*, 199–211. [CrossRef]
37. Cuccovillo, T.; Coop, M.R. On the mechanics of structured sands. *Géotechnique* **1999**, *49*, 741–760. [CrossRef]
38. Consoli, N.C.; Cruz, R.C.; Da Fonseca, A.V.; Coop, M.R. Influence of cement-voids ratio on stress-dilatancy behavior of artificially cemented sand. *J. Geotech. Geoenvironmental Eng.* **2012**, *138*, 100–109. [CrossRef]
39. Airey, D.W. Triaxial testing of naturally cemented carbonate soil. *J. Geotech. Eng.* **1993**, *119*, 1379–1398. [CrossRef]
40. Coop, M.R.; Willson, S.M. Behavior of hydrocarbon reservoir sands and sandstones. *J. Geotech. Geoenvironmental Eng.* **2003**, *129*, 1010–1019. [CrossRef]